Dyes and Pigments 92 (2011) 674–680

Contents lists available at ScienceDirect

Dyes and Pigments

journal homepage: www.elsevier.com/locate/dyepig

Novel red-emitting thieno-[3,4-*b*]-pyrazine derivatives suitable for vacuum evaporation and solution method to fabricate non-doped OLEDs

Qing Li [a], Jiuyan Li [b], Ruixia Yang [a], Lijun Deng [b], Zhanxian Gao [a], Di Liu [a,*]

[a] School of Chemistry, Dalian University of Technology, 2 Linggong Road, Dalian 116024, China
[b] State Key Laboratory of Fine Chemicals, School of Chemical Engineering, Dalian University of Technology, 2 Linggong Road, Dalian 116024, China

ARTICLE INFO

Article history:
Received 11 April 2011
Received in revised form
31 May 2011
Accepted 31 May 2011
Available online 15 June 2011

Keywords:
Thieno-[3,4-*b*]-pyrazine
Red
Organic light-emitting diodes
Solution processing
Vacuum evaporation
Large Stokes shift

ABSTRACT

Two novel red-emitting thieno-[3,4-*b*]-pyrazine-cored molecules with phenyls (**TP**) or polyphenyls (Müllen type dendron, **DTP**) as peripheral groups were designed and synthesized. They have large Stokes shifts over 100 nm. **DTP** is thermally stable with decomposition temperature up to 458 °C. More importantly, it is amorphous with a remarkably high glass transition temperature of 262 °C. **DTP** can be made into thin films either by solution method or vacuum evaporation. Red OLEDs were fabricated using either spin coated or vacuum evaporated **DTP** film as emitting layer. The evaporated device exhibited a maximum brightness of 1753 cd m^{-2} and a luminous efficiency of 0.74 cd A^{-1}, which are among the best data ever reported for thieno-[3,4-*b*]-pyrazine derivatives so far. In contrary, **TP** failed to produce satisfied red emission in its evaporated OLEDs.

1. Introduction

Organic light-emitting devices (OLEDs) have been drawing broad attentions due to their practical applications in both large-area flat-panel displays and solid-state lighting. For light-emitting materials used in OLEDs, to possess a large Stokes shift is usually an essential merit if an efficient light output from the device is desired, since otherwise the severe self-absorption due to spectral overlap between the absorption and emission will definitely be unfavorable to light output [1]. Among the three primary color light-emitting materials and devices, the red one still lag behind in terms of luminescent efficiency and lifetime [2–4]. It is strongly desired that, therefore, highly efficient red emitters with good merits such as a large Stokes shift are developed for application in OLEDs. Thieno-[3,4-*b*]-pyrazine is a typical red fluorophore which is characterized by pure and saturated red emission and large Stokes shifts over 110 nm. There are two major absorption bands for this chromophore, one narrow but strong band centered at 320 nm and another broad but weak one covering from 450 to 530 nm. The weak absorption at longer wavelength range has a tiny overlap with the fluorescence, leading to negligible self-absorption and efficient light output. As far as we know, however, only few thieno[3,4-*b*] pyrazine based materials have been developed for application as emitters in OLEDs to date [4].

The thieno-[3,4-*b*]-pyrazine chromophore has a nearly planar conformation due to π conjugation of the two aromatic rings. It is well known that strong intermolecular interaction exists in the solid states of organic molecules, especially of the planar molecules, which usually results in unwanted effects such as fluorescence quenching and spectral contamination. Therefore, in order to suppress the intermolecular interaction to gain pure red emission with satisfactory performance in the solid state, it is necessary to decorate the flat thieno-[3,4-*b*]-pyrazine chromophore with bulky functional groups so that it can act as efficient solid emitter. Based on the chemical structure of thieno-[3,4-*b*]-pyrazine, the modification groups can be easily grafted to its 2,3,5,7-positions. The molecules designed in this way should have three-dimension non-planar conformation with the planar emissive core encapsulated by the surrounding bulky groups.

In this paper, we report the design and synthesis of two novel thieno-[3,4-*b*]-pyrazine based molecules, **TP** and **DTP** (Scheme 1). For **TP**, Four phenyls were attached to the 2,3,5,7-positions of the thieno-[3,4-*b*]-pyrazine emissive core as the periphery groups. While for **DTP**, much larger tetraphenylphenylenes (i.e., polyphenyl, Müllen type dendron) were introduced through a phenylene bridge into the 2,3,5,7-positions of thieno-[3,4-*b*]-pyrazine core as bulky arms, in order to protect the core via site-isolation effect, and to

* Corresponding author. Tel./fax: +86 411 84986233.
E-mail address: liudi@dlut.edu.cn (D. Liu).

0143-7208/$ – see front matter © 2011 Elsevier Ltd. All rights reserved.
doi:10.1016/j.dyepig.2011.05.029

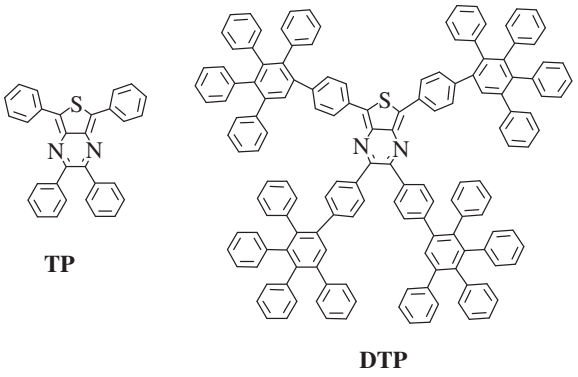

Scheme 1. Chemical structures of **TP** and **DTP**.

generate the thermally and morphologically stable molecule due to the excellent stability of this type of group [5,6]. In addition, the presence of these periphery groups helps to provide significant molecular weight and good solubility, so that the resultant **DTP** is capable of being processed by solution methods to form thin films and OLEDs. To be suitable for solution processing is well accepted as one essential merit for light-emitting materials since the solution processing is the most favorable fabrication technique of OLEDs for practical applications in low-cost, large-area flat-panel displays and solid-state lighting [7,8]. In comparison with **TP**, the **DTP** molecule is expected to have the advantageous features including high fluorescent quantum yield in solid state with large Stokes shift, being suitable for solution processing, and good thermal stability for vapor deposition for non-doped OLEDs. The photophysical, electrochemical and electroluminescent properties of **TP** and **DTP** are investigated. The results show that **DTP** is a more efficient solid emitter in comparison with **TP**. More importantly, **DTP** has the flexibility to be processed either by solution method such as spin coating or by vacuum evaporation to fabricate OLEDs. A brightness of 428 cd m^{-2} was obtained for the spin coated OLEDs. While for the OLED in which all organic layers were vacuum evaporated, the hole transporting layer was utilized and the device performance was greatly improved with a maximum brightness of 1753 cd m^{-2} and a luminous efficiency of 0.74 cd A^{-1}. This performance is among the best data ever reported for thieno-[3,4-*b*]-pyrazine derivatives so far.

2. Experimental

2.1. Materials and instruments

All the chemicals and reagents for the synthesis are of analytical grade and used as received from commercial sources without further purification. ^{1}H NMR spectra were recorded on a Bruker Avance II (400 MHz) and Varian INOVA spectrometer (400 MHz). Mass spectra were recorded on a GC–TOF-MS (Micromass, UK) mass spectrometer for TOF-MS-EI, a MALDI micro MX (Waters, USA) for MALDI-TOF-MS and HP 1100 LC-MSD (USA) mass spectrometer. The fluorescence and UV–vis absorption spectra measurements were performed on a Perkin–Elmer LS55 fluorescence spectrometer and a Perkin–Elmer Lambda 35 UV–Visible spectrophotometer, respectively. The fluorescence quantum yields were determined in CH_2Cl_2 or toluene solutions against rhodamine B as the standard ($\Phi = 0.97$ in ethanol) [9,10]. Melting points (Mp.) were recorded on a WRS-1B digital melting point instrument (Shanghai Precision and Scientific Instrument Co.)

2.2. Cyclic voltammetry measurements

Electrochemical measurements were performed by using a conventional three-electrode configuration and an electrochemical workstation (BAS100B, USA) at a scan rate of 50 mV s^{-1}. A glass carbon working electrode, a Pt-wire counter electrode, and a saturated calomel electrode (SCE) as reference electrode were used. All measurements were made at room temperature on samples dissolved in CH_2Cl_2, with 0.1 M tetra-n-ethylammonium tetrafluoroborate as supporting electrolyte. From the values of the onset oxidation (E_{ox}^{onset}) and reduction potentials (E_{red}^{onset}) relative to the saturated calomel electrode (SCE) electrode, the energies of the highest occupied molecular orbital (HOMO) and the lowest unoccupied molecular orbital (LUMO) as well as the electrochemical band gaps (E_g^{CV}) of **DTP** were calculated according to the equations below (Eqs. (1)–(3)) [11–13]:

$$\text{HOMO} = -e\left(E_{ox}^{onset} + 4.4\right)\ [\text{eV}] \quad (1)$$

$$\text{LUMO} = -e\left(E_{red}^{onset} + 4.4\right)\ [\text{eV}] \quad (2)$$

$$E_g^{CV} = e\left(E_{ox}^{onset} - E_{red}^{onset}\right)\ [\text{eV}] \quad (3)$$

2.3. OLED fabrication and measurements

The pre-cleaned ITO glass substrates were treated by UV-ozone for 20 min. A 40 nm thick PEDOT:PSS film was first deposited on the ITO glass substrates, and baked at 120 °C for 40 min in air. In type I device, the emitting layer were spin coated from the solution of **DTP** in chlorobenzene on the top of PEDOT:PSS film. In type II device, the **DTP**, **TP** film and other organic layers were deposited by vacuum evaporation in a vacuum chamber with a base pressure less than 10^{-6} Torr. Finally a thin layer of LiF (1 nm) and 100 nm of Al were vacuum deposited on top of organic layers as cathode. PEDOT:PSS (poly(3,4-ethylenedioxythiophene):poly(styrene sulfonate)) acts as the hole injecting and transporting layer, NPB (4,4′-bis [N-(1-naphthyl)-N-phenylamino]biphenyl) acts as the hole transporting layer, TPBI (2,2′,2″-(1,3,5-benzenetriyl)tris(1-phenyl-1H-benzimidazole))as the electron-transporting layer, ITO (indium tin oxide) and LiF/Al as anode and cathode respectively. The film thickness in above configuration is chosen after optimization. The EL spectra, CIE coordinates, and current–voltage–luminance characteristics were measured with computer-controlled Spectrascan PR 705 photometer and a Keithley 236 source-measure-unit. All the measurements were carried out at room temperature under ambient conditions.

2.4. Synthesis of compounds

2,5-dibromo-3,4-dinitrothiophene (**1**): Concentrated sulfuric acid (100 ml) and fuming sulfuric acid (30% SO_3, 100 ml) were combined in a flask equipped with a mechanical stirrer and cooled with an ice bath. 2,5-dibromothiophene (53.8 g, 0.222 mol) was then added at a temperature below 20 °C. Concentrated nitric acid (35 ml) was then added carefully to keep the temperature under 30 °C. Once the addition was completed, the mixture was allowed to react for an additional 3 h and then poured over 800 g of ice. Upon the melting of the ice, the solid residue was recovered by vacuum filtration and washed well with water to produce a light yellow powder. Recrystallization with methanol gave 69.3 g (94%) of analytically pure material; Mp. 135.8–136.7 °C.

2,5-Bis-phenyl-3,4-dinitro-thiophene (**2a**) and *2,5-Bis-(4-bromophenyl)-3,4-dinitro-thiophene* (**2b**): To a mixture of compound **1** (5 g, 15 mmol), phenylboronic acid or 4-bromophenylboronic acid (33 mmol) and [$Pd(PPh_3)_4$] (450 mg, 375 mmol) were added under nitrogen 250 ml toluene, 50 ml methanol and 65 ml K_2CO_3 aqueous (2 M) solution. The reaction mixture was refluxed for 8 h and then

diluted with water. The organic layer was separated, and the aqueous layer was extracted with CH_2Cl_2 (3 × 50 ml). After washed with brine (1 × 50 ml) and dried over $MgSO_4$, the CH_2Cl_2 extraction was combined with the original organic reaction solution. The resulted organic solution was evaporated under reduced pressure and the residue was purified by column chromatography over silica gel with mixed petroleum ether and CH_2Cl_2 (2:1 v/v) as eluent to give yellow solid. **2a**: yield 37%, was used directly for synthesis of **3a**.

2b: yield 41.2%. ^{1}H NMR (400 MHz, $CDCl_3$): $\delta = 7.65$ (d, $J = 8.0$ Hz, 4H; Ar-H), 7.39 (d, $J = 8.0$ Hz, 4H; Ar-H); MS (TOF-MS-EI, m/z): Calcd. for $C_{16}H_8Br_2N_2O_4S$: 481.86; found 481.86.

2,5-Bis-phenyl-3,4-thiophene-3,4-diamine (**3a**) and *2,5-Bis-(4-bromo-phenyl)-3,4-thiophene-3,4-diamine* (**3b**): To a suspend of **2a** or **2b** (10 mmol) and tin powder (9.4 g, 800 mmol) in ethanol (150 ml) was added concentrated HCl acid and the mixture was subsequently stirred under nitrogen at 50 °C for 6 h. The homogeneous solution was poured into ice water and made alkaline with aqueous NaOH. The organic layer was separated, and the aqueous layer was extracted with CH_2Cl_2 (3 × 50 ml) and the dried extraction was combined with the original organic solution. The organic mixture was evaporated under reduced pressure. The white solid was recrystallized from CH_2Cl_2/petroleum ether (2:1 v/v) to yield an analytically pure sample. **3a**: yield 80.2%, not characterized.

3b: yield 85.2%. MS (TOF-MS-EI, m/z): Calcd. for $C_{16}H_{12}Br_2N_2S$, 421.91; found 421.91.

2,3-Bis-phenyl-5,7-bis-phenyl-thieno[3,4-b]pyrazine (**TP**) and *2,3-Bis-(4-bromo-phenyl)-5,7-bis(4-bromo-phenyl)-thieno[3,4-b]pyrazine* (**4**): Compound **3** (1 mmol) and 1,2-bis-phenyl-ethane-1,2-dione or 1,2-bis-(4-bromo-phenyl)-ethane-1,2-dione (1 mmol) were dissolved in dry $CHCl_3$ (60 ml) and a catalytic amount of *p*-toluenesulfonic acid was added. The mixture was stirred at room temperature overnight. The red solid were collected by filtration and dried under vacuum. Recrystallization with $CHCl_3$/petroleum ether (3:1 v/v) gave analytically pure material.

TP: yield 65.1%. ^{1}H NMR (400 MHz, $CDCl_3$): $\delta = 8.3$ (d, 4H, $J = 8.0$ Hz; Ar-H), 7.56 (d, 4H, $J = 8.0$; Ar-H), 7.51 (t, 4H; Ar-H), 7.37–7.33 (m, 8H, Ar-H); MS (TOF-MS-EI, m/z): Calcd. for $C_{30}H_{20}N_2S$, 440.13; found 440.13. Elemental anal. calc. for $C_{30}H_{20}N_2S$: C, 81.79; H, 4.58; N, 6.36. Found: C, 81.34; H, 4.63; N, 6.21.

4: yield 84.3%. ^{1}H NMR (400 MHz, $CDCl_3$): $\delta = 8.13$ (d, 4H, $J = 7.6$ Hz; Ar-H), 7.63 (d, 4H, $J = 8.0$ Hz; Ar-H), 7.53 (d, 4H, $J = 8.0$ Hz; Ar-H), 7.40 (d, 4H, $J = 7.6$ Hz; Ar-H); MS (TOF-MS-EI, m/z): Calcd. for $C_{30}H_{16}Br_4N_2S$, 751.78; found 751.78.

2,3-Bis-(4-(trimethylsilylethynyl)phenyl)-5,7-bis-(4-(trimethylsilyl) ethynylphenyl)-thieno[3,4-b]pyrazine (**5**): Compound **4** (500 mg, 0.67 mmol) was dissolved in a degassed mixture of triethylamine (20 mL) and absolute THF (10 mL) under nitrogen. [$PdCl_2(PPh_3)_2$] (93 mg, 5 mol%), CuI (63 mg, 0.33 mmol), and PPh_3 (86 mg, 0.33 mmol) were then added under a flow of nitrogen. After the flask was sealed with a septum, trimethylsilylethyne (0.45 ml) was injected. The reaction mixture was stirred at 45 °C for 48 h, and then poured into an equal volume of CH_2Cl_2 and filtered. The solvent was removed and the crude product was purified by column chromatography over silica gel with mixed petroleum ether and CH_2Cl_2 (2:1 v/v) as eluent to give red solid (400 mg, 73.4%). ^{1}H NMR (400 MHz, $CDCl_3$): $\delta = 8.23$ (d, 4H, $J = 8.4$ Hz; Ar-H), 7.56 (d, 4H, $J = 8.4$ Hz; Ar-H), 7.46–7.41 (q, 8H; Ar-H), 0.278 (s, 18H; CH_3), 0.271(s, 18H; CH_3); MS (MALDI-TOF, m/z): Calcd. for $C_{50}H_{52}N_2SSi_4$, 824.29; found 824.18.

2,3-Bis-(4-ethynyl-phenyl)-5,7-bis(4-ethynyl-phenyl)-thieno[3,4-b]pyrazine (**6**): Compound **5** (400 mg, 0.48 mmol) and NH_4F (143 mg, 3.9 mmol) were dissolved in THF (10 mL) under nitrogen. A solution of *n*-Bu_4NF (19 mg, 0.07 mmol) in THF (5 mL) was added by injection. The mixture was stirred at room temperature for 2 h. Then the solvents were removed in vacuum, and the crude product was purified by column chromatography over silica gel with mixed petroleum ether and CH_2Cl_2 (3:1 v/v) as eluent to give a red solid **6** (255 mg, 98%). ^{1}H NMR (400 MHz, $CDCl_3$): $\delta = 8.27$ (d, 4H, $J = 8.4$ Hz; Ar-H), 7.61 (d, 4H, $J = 8.4$ Hz; Ar-H), 7.48 (s, 8H; Ar-H), 3.19 (s, 2H; C≡CH), 3.17(s, 2H; C≡CH); MS (TOF-MS-EI, m/z): Calcd. for $C_{38}H_{20}N_2S$, 536.13; found 536.13.

DTP: Compound **6** (200 mg, 0.37 mmol) and **7** (1.79 mmol) in 10 ml *o*-xylene were stirred and refluxed for 72 h under nitrogen.

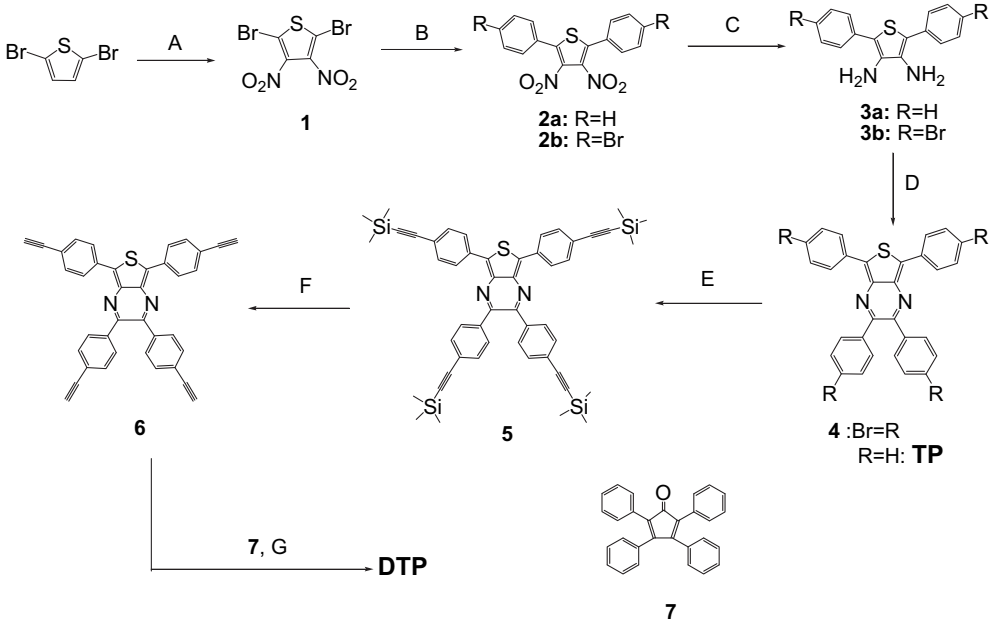

Scheme 2. Synthetic routes for **TP** and **DTP**. Conditions and reagents; A) fuming H_2SO_4, conc. HNO_3, r.t.; B) phenylboronic acid or 4-bromophenylboronic acid, $Pd(PPh_3)_4$, K_2CO_3, toluene, MeOH, reflux, N_2; C) Sn, conc. HCl, EtOH, 50 °C, N_2; D) *p*-toluenesulfonic acid, dry $CHCl_3$, 1,2-diphenylethane-1,2-dione or 1,2-bis(4-bromophenyl)ethane-1,2-dione, r.t.; E) NEt_3, $PdCl_2(PPh_3)_2$, PPh_3, CuI, THF, trimethylsilylethyne, 45 °C, N_2; F) NH_4F, *n*-Bu_4NF, THF, r.t., N_2; G) *o*-xylene, compound **7**, reflux, N_2.

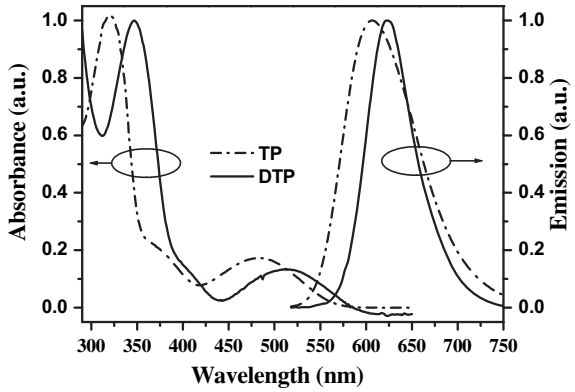

Fig. 1. UV–vis absorption and photoluminescence (PL) spectra of **TP** and **DTP** in CH_2Cl_2 solutions (10^{-5} mol L^{-1}, $\lambda_{exc} = 470$ nm).

After cooling to room temperature, the solvent was evaporated under reduced pressure. The crude product was purified by column chromatography over silica gel with mixed petroleum ether and CH_2Cl_2 (3:2 v/v) as eluent and then recrystallization to give pure product as red powder, yield 77.5%. ^{1}H NMR (400 MHz, $CDCl_3$): $\delta = 8.05$ (d, 4H, $J = 8.0$ Hz; Ar-H), 7.62 (d, 4H, $J = 12.0$ Hz; Ar-H), 7.25–7.23 (d, 4H, $J = 8.0$ Hz; Ar-H), 7.17 (d, 20H, $J = 4.0$ Hz; Ar-H), 7.09 (d, 4H, $J = 8.0$ Hz; Ar-H), 6.97–6.92 (m, 20H; Ar-H), 6.91–6.82 (m, 32H; Ar-H), 6.80–6.77 (m, 12H; Ar-H); MS (MALDI-TOF, *m*/*z*): Calcd. for $C_{150}H_{100}N_2S$, 1960.76; found 1961.1299, 1962.1105, 1963.1215. Elemental anal. calc. for $C_{150}H_{100}N_2S$: C, 91.80; H, 5.14; N, 1.43. Found C, 91.42; H, 5.26; N, 1.35.

3. Results and discussion

3.1. Synthesis

The synthetic procedures for **TP** and **DTP** are shown in Scheme 2. The thieno[3,4-*b*]-pyrazine emissive core was easily formed by cyclizative condensation of 2,5-diaryl-3,4-diaminothiophene and 1,2-diarylethane-1,2-dione in the presence of *p*-toluenesulfonic acid. The four terminal ethynyl groups were grafted at the periphery of the key intermediate **6** to serve as the reaction sites to introduce the polyphenyl arms. The polyphenyl groups were constructed through Diels–Alder cycloaddition of tetraphenylcyclopentadienones **7** to the terminal ethynyl groups in **6**. The Diels–Alder cycloaddition was carried out for a significantly long time under an atmosphere of nitrogen to ensure the complete conversion of all ethynyl groups and thus a high yield (77.5%) of the product. **DTP** is well soluble in common organic solvents such as CH_2Cl_2, tetrahydrofuran, ethylacetate, so that it was easily isolated and purified by column chromatography and recrystallization to reach an excellent purity for OLEDs application. In contrast, **TP** is not as easily soluble as **DTP** in same solvent. The chemical structure and the monodispersity of **DTP** were verified using ^{1}H NMR spectroscopy, and matrix-assisted laser desorption ionization time-of-flight (MALDI-TOF) mass spectrometry. Based on the good solubility and the significant molecular weight of **DTP**, good-quality thin films (Fig. S1 in Supporting information) can be formed by spin coating its chlorobenzene solution, which makes it possible to use wet method for **DTP** to fabricate OLEDs.

3.2. Photophysical properties

The photophysical properties of **TP** and **DTP** were examined by UV–vis absorption and photoluminescence (PL) spectra in CH_2Cl_2 and toluene solutions. As shown in Fig. 1, they exhibit two major electronic absorption bands: π–π^* transition at 345–350 nm and charge transfer (CT) transition at 515–520 nm [4,8]. It is obvious that the absorption spectra of **DTP** exhibits a red shift of 30 nm compared with that of the reference compound **TP**, which should be assigned to the extended π conjugation in **DTP** molecules. It should be noted that the absorption intensity of the long-wavelength band is much lower than the short wavelength range for both thienopyrazine-based compounds. As illustrated by the emission spectra in Fig. 1 and the data in Table 1, **DTP** transmits red fluorescence in both non-polar solvents such as toluene and polar solvents such as CH_2Cl_2 upon photoexcitation at room temperature. The structureless emission spectra remains unaltered irrespective of the excitation wavelength, which is possibly due to an efficient relaxation to the lowest excited state [4]. This CT emission exhibits a moderate positive solvatochromism. For instance, emission peak of **DTP** moves from 613 nm in toluene to 623 nm in CH_2Cl_2. In dilute solutions of CH_2Cl_2, the parent compound **TP** exhibits orange red fluorescence with the emission peak at 605 nm, while the emission spectra for **DTP** is red shifted with a peak at 623 nm. Furthermore, the full width at half maximum (FWHM) in the PL spectra is 60 and 93 nm for **DTP** and **TP**, respectively. The observed spectra narrowing for **DTP** should be attributed to the fact that the intermolecular interaction is dramatically eliminated due to the site-isolation effect of the bulky polyphenyl arms. It is evident that both the red shift and the spectral narrowing due to the introduction of the polyphenyl groups are definitely favorable to obtain the pure and saturated red fluorescence for **DTP**. The parent compound **TP** exhibits a moderate fluorescent quantum yield of 60.5% in toluene. However, it decreases to 28.4% in CH_2Cl_2. This dipolar quenching phenomena is frequently observed for organic compounds due to their interaction with a polar solvent [4]. While **DTP** shows a fluorescent quantum yield of 43.6% in dilute toluene solution. It is reasonable that the fluorescent quantum yield of **DTP** is slightly decreased in comparison with **TP**, since the non-irridiative decay efficiency is increased due to the presence of more chemical groups within this molecule. The decrease in fluorescence quantum yield for **DTP** will be acceptable if the comprehensive properties of this material are taken into account.

As shown in Fig. 1, there is little overlap between the absorption and emission spectra of these thieno-[3,4-*b*]-pyrazine derivatives. Calculated from the positions of the long-wavelength absorption maximum and the fluorescence maximum, the Stokes shifts for

Table 1
Photophysical and electrochemical data of **TP** and **DTP**.

	λ_{abs} (nm)	λ_{em} (nm)	Φ (%)[a]	Stokes shift (nm)	HOMO/LUMO (eV)	E_g^{optb} (eV)	E_g^{CVc} (eV)
	Toluene/CH_2Cl_2	Toluene/CH_2Cl_2	Toluene/CH_2Cl_2	Toluene/CH_2Cl_2			
TP	323, 488/320, 482	597/605	60.5/28.4	109/123	−/−3.18		
DTP	350, 519/346, 518	613/623	43.6/25.1	94/105	−5.41/−3.42	2.04	1.99

[a] Related to rhodamine B as the standard ($\Phi = 0.97$ in ethanol).
[b] Optical band gap, determined from absorption onset.
[c] Electrical band gap, determined by subtracting LUMO energy from that of HOMO.

these compounds are as large as 105–123 nm in CH_2Cl_2. Such a large Stokes shift is especially valuable for light-emitting materials used in non-doped OLEDs since each emissive molecule is densely surrounded in the neat film and the absence of self-absorption will definitely facilitate efficient light output from the device.

3.3. Thermal properties

The thermal properties of **TP** and **DTP** were examined by differential scanning calorimetry (DSC) and thermogravimetric analysis (TGA) at a scanning rate of 10 °C min^{-1}. The TGA and DSC thermograms for **DTP** are illustrated in Figs. S2 and S3 in Supporting information. In TGA measurement, the decomposition temperature of **DTP** was determined as 506 °C, indicating the excellent thermal stability of this compound. This is an essential merit for organic light-emitting materials especially when they are used under high temperature. The thermal stability is suggested to benefit from the presence of the polyphenyl groups, which is famous for its excellent thermal and chemical stabilities [14]. The morphological stability of **DTP** was monitored by DSC measurement. When a powder of **DTP** obtained from organic solvent is heated for the first run, an endothermic peak at 262 °C was first observed, which should be ascribed to the glass transition process. Upon further heating beyond this glass transition temperature (T_g), an exothermal peak was detected at 288 °C (T_c), which is assigned to the crystallization. With further increasing the temperature, the crystal state melts into the isotropic liquid at 444 °C (T_m). The isotropic liquid was rapidly cooled into the glassy state. In the second heating run, the glass transition was repeated at the same temperature. The detection of the glass transition in the first heating run implies that **DTP** is quite ready to form the glassy state even when it is obtained directly from organic solvents. This is in contrast to most organic compounds that usually crystallize when they separate out from liquid solvents. Such a high T_g of 262 °C indicates a high amorphous stability of **DTP** in solid state, which should benefit from the non-planar configuration of this molecule due to the presence of the bulky polyphenyl groups [15]. A high T_g is one essential merit for light-emitting materials used in OLEDs since a morphologically stable amorphous organic layer usually leads to a longer lasting OLED [12]. In principle, all the organic layers forming the OLED devices should have T_g as high as possible. The individual layer that has the lowest T_g is likely to limit the thermal stability of the OLED. In comparison with **DTP**, the reference compound **TP** has a much lower melting point (T_m) of 263 °C. Evidently the introduction of the polyphenyl arms in **DTP** molecule resulted in the excellent thermal and amorphous stability of this material. Due to the excellent thermal stability, it is observed that **DTP** is suitable for vacuum evaporation to form good-quality thin films at a proper temperature without decomposition.

3.4. Electrochemical properties

The redox behavior of these thieno[3,4-*b*]pyrazine derivatives was investigated by means of cyclic voltammetry measurements. As shown by the cyclic voltammograms in Fig. 2, the reference compound **TP** exhibits two reversible reduction waves, which should be assigned to two step one-electron reductions of the thieno-[3,4-*b*]-pyrazine core. No oxidation was observed for it. The detection of only reduction processes indicates the electron-deficient and n-type feature of the thieno-[3,4-*b*]-pyrazine chromophore, despite that most thiophene-containing species usually reveal electron-donating and p-type nature [4,16,17]. With introduction of the polyphenyl arms, multiple oxidation waves were detected in addition to the reduction waves for **DTP**. It would be safe to assign the reduction to the thieno-[3,4-*b*]-pyrazine core and the oxidation to the polyphenyl groups. From the values of E_{ox}^{onset} and E_{red}^{onset}, the energies of the highest occupied molecular orbital (HOMO) and the lowest unoccupied molecular orbital (LUMO) as well as the electrochemical band gaps (E_g^{CV}) of **DTP** were calculated.

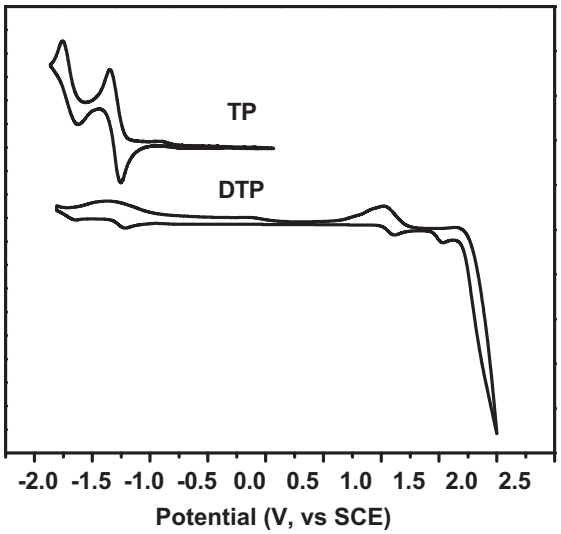

Fig. 2. Cyclic voltammograms of **TP** and **DTP** (scan rate 50 mV S^{-1}, in CH_2Cl_2).

The optical band gap (E_g^{opt}) of **DTP** was also determined by absorption edge technique for its film. The E_g^{opt} was calculated as 2.04 eV, which is quite close to the electrochemical band gap E_g^{CV}. The consistence of this parameter obtained from two different methods implies the high accuracy of these experimental methods. All the electronic data are listed in Table 1.

3.5. Electroluminescence

In order to evaluate the electroluminescent properties, **TP** and **DTP** were used as the neat emitting layer (EML) to fabricate non-doped OLEDs. Based on the excellent solubility of **DTP** in common organic solvents, high quality neat films without pinholes can be obtained by spin coating its solution in chlorobenzene. Therefore, two types of devices were fabricated by spin coating the **DTP** layer: ITO/PEDOT:PSS (40 nm)/**DTP** (25 nm)/BCP (10 nm)/Alq_3 (30 nm)/LiF (1 nm)/Al (100 nm) (device A), and ITO/PEDOT:PSS (40 nm)/**DTP** (25 nm)/TPBI (40 nm)/LiF (1 nm)/Al (100 nm) (device B). In device A, PEDOT:PSS (poly(3,4-ethylenedioxythiophene):poly(styrene sulfonate)) was used as the hole injecting layer, BCP (2,9-dimethyl-4,7-diphenyl-1,10-phenanthroline) as hole-blocking layer, Alq_3 (tris(8-hydroxyquino) aluminum) as the electron-transporting layer. For performance optimization purpose, TPBI (1,3,5-tris[N-(phenyl) benzimidazole]-benzene) was used as both hole-blocking and electron-transporting layer in device B. These two OLEDs were fabricated by spin coating the PEDOT:PSS and **DTP** layers and then thermally evaporating other organic layers and cathode in a vacuum chamber.

Both device A and B exhibited saturated red electroluminescence (EL) with emission peak at 646 nm. The EL spectra of both devices are identical to each other regardless of the difference in device configuration. This indicates that both BCP and TPBI layers played essential role to well confine holes and excitons within the **DTP** emitting layer and the red EL is obtained exclusively from the **DTP** molecules without contamination from any interface emission. As shown in Fig. 3, the EL spectra are red shifted and broadened if

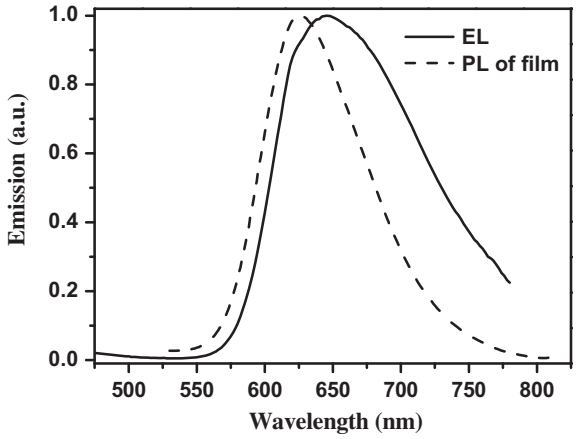

Fig. 3. The PL spectrum of **DTP** film and the EL spectrum of **DTP** based OLEDs.

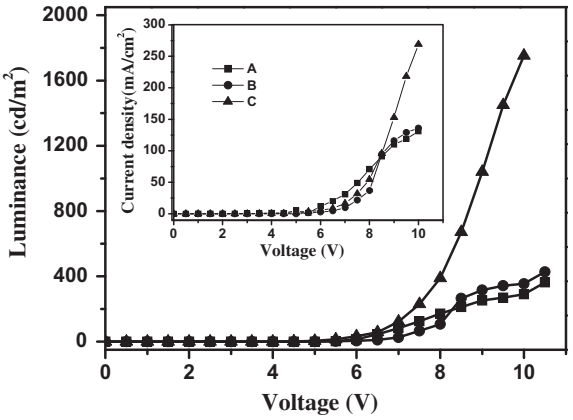

Fig. 4. Luminance–voltage (L–V) curves of OLEDs A, B, and C. Insert: current density–voltage (J–V) curves of the three OLEDs.

compared to the PL spectra of the **DTP** film. This is frequently observed in OLEDs due to the effect of the electrical field on the excited states of organic molecules. The EL spectra correspond to coordinates on the 1931 CIE chromaticity diagram of (0.65, 0.33). This is close to (0.64, 0.33), which are the coordinates of the standard red color of the National Television System Committee (NTSC) [9]. Moreover, the EL spectra and CIE coordinates of both device A and B almost keep unchanged with increasing driving voltage, which offers better device operation compared to red OLEDs with dopants in which the color changes with voltage [18]. Both device A and B turned on (to deliver a brightness of 1 cd/m^2) at 5.5 V. A maximum brightness of 362 cd m^{-2} and a peak luminance efficiency of 0.26 cd A^{-1}, and 428 cd m^{-2} and 0.30 cd A^{-1} were obtained for device A and B, respectively. Obviously the performance of these two OLEDs containing spin coated **DTP** layer are not as satisfied as expected. This is probably due to the absence of hole transporting layer and the non-balance of hole and electron charges in the emitting layers in these devices.

In order to optimize the EL performance of **DTP** based device, the third type of OLED was fabricated in which a hole transporting layer was introduced between the anode and the **DTP** emitting layer. The configuration of device C is as follows: ITO/NPB (40 nm)/**DTP** (25 nm)/TPBI (40 nm)/LiF (1 nm)/Al (100 nm). NPB (4,4′-bis[N-(1-naphthyl)-N-phenylamino]biphenyl) was used as the hole transporting layer to increase the hole current and thus to improve the charge balance in the emitting layer. Device C was fabricated by thermal evaporating all organic layers and cathode in vacuum. As shown by the data in Table 2, the EL spectra and CIE coordinates of device C are identical to those of device A and B. Fig. 4 illustrates the curves of current density and luminance versus voltage for these three OLEDs. Device C turned on at a much lower voltage (4.5 V) than both device A and B. Furthermore, the current at a given voltage is higher for device C than device B, especially at high driving voltage range. The only difference in device configuration between device B and C should be responsible for their different current density. It would be safe to conclude that the introduction of NPB layer in device C greatly improved the device current. As a result, the brightness at a given voltage of the device C is substantially higher than other two devices. A maximum brightness of 1753 cd m^{-2} (at 10 V) was obtained for device C. Fig. 5 compares the luminance efficiencies curves for these three types of OLEDs. It is apparent that the device C is much superior to other two devices and a maximum luminance efficiency of 0.74 cd A^{-1} at 20 mA cm^{-1} was obtained. The luminance efficiency almost keeps constant even up to a high current density of 270 mA cm^{-1}. The maximum external quantum efficiency was calculated as 0.44%. The substantially improved emission efficiency in device C indicates that the introduction of the NPB hole transporting layer improved the positive and negative charge balance and consequently favored the efficient charge recombination and light emission. It should be noted that the vacuum evaporated **DTP** film probably have better film quality than the spin coated one, which may be a possible reason for the improved device performance of device C than device B.

As stated in literatures, the thieno-[3,4-*b*]-pyrazine derivative in previous report [4] could reach a maximum luminance efficiency of 0.34 cd A^{-1} and brightness of 1766 cd m^{-2} with CIE (0.65, 0.33). A higher efficiency of 0.65 cd A^{-1} was possible but at the expense of the emission color shifting to orange (0.59, 0.33). Evidently **DTP** has higher emission efficiency than the reported counterparts on the premise of saturated red emission. To the best of our knowledge, a luminance efficiency of 0.74 cd A^{-1} of our present red OLEDs is the

Table 2
Device performance of **DTP** based OLEDs A, B and C.

Devices	V_{on} (V)	L_{max} (cd/m^2) [at the voltage (V)]	η_{max} (cd/A) [at mA/cm^2]	η(cd/A) [at 100 mA/cm^2]	λ_{max} (nm)	CIE(x, y)
A	5.5	362 (11)	0.26 (31.0)	0.23	646	0.65, 0.33
B	5.5	428 (10.5)	0.30 (17.9)	0.28	646	0.65, 0.33
C	4.5	1753 (10)	0.74 (16.5)	0.70	646	0.65, 0.33

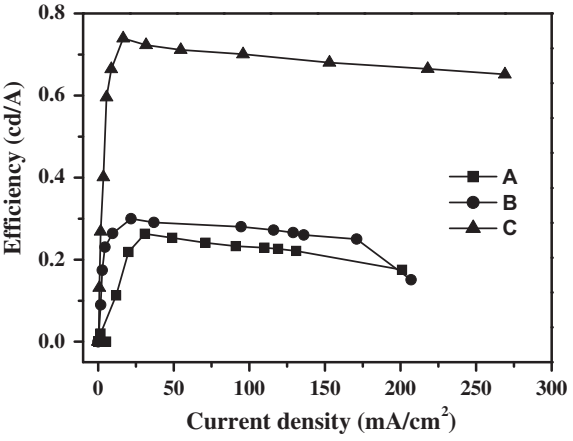

Fig. 5. Plots of the luminance efficiency versus current density for OLEDs A, B and C.

best efficiency ever reported for thieno-[3,4-*b*]-pyrazine derivatives so far.

In contrast to the good performance of **DTP**, the OLEDs containing the evaporated **TP** emitting layer with similar structure to device A always produced a mixed emission from both **TP** and Alq_3 (Fig. S4 in Supporting information) with poor intensity, although great efforts were taken to tune the thickness of each functional layer. Alternatively the **TP** based OLEDs with similar configuration to device B produced extremely weak emission. This may result from the unbalanced charge transporting processes within the devices and the strong unwanted intermolecular interaction of more planar **TP** molecules in solid states. Once again it implies that the bulky polyphenyl groups in **DTP** molecules indeed play essential role to improve its emission performance.

4. Conclusions

We have demonstrated that attaching bulky polyphenyl groups at the periphery of the planar thieno-[3,4-*b*]-pyrazine chromophore produced the efficient solid-state emitter. The generated thieno-[3,4-*b*]-pyrazine derivative, **DTP**, has good solubility, excellent thermal and amorphous stabilities. It is characterized by the flexibility to be made into thin films and OLEDs either by spin coating or vacuum evaporation technique. Non-doped OLEDs containing either spin coated or vacuum evaporated **DTP** film as emitting layer were fabricated and they all exhibited saturated red emission with CIE coordinates of (0.65, 0.33). In the vacuum evaporated OLED, due to the utilization of the hole transporting layer and the improved **DTP** film quality by vacuum deposition, the device performance are much superior to those of the spin coated devices. A maximum brightness of 1753 cd m^{-2} and a peak luminance efficiency of 0.74 cd A^{-1} were obtained for the vacuum evaporated red OLEDs. This report provides a practical strategy to decorate the highly efficient but planar luminophor to be efficient solid emitter suitable for application in non-doped OLEDs.

Acknowledgments

We thank the National Natural Science Foundation of China (20704002, 21072026 and U0634003), the Ministry of Education for the New Century Excellent Talents in University (Grant NCET-08-0074), the NKBRSF (2009CB220009), the Fundamental Research Funds for the Central Universities (DUT10LK16), and the Key Laboratory of Photochemical Conversion and Optoelectronic Materials (TIPC, CAS) for financial support of this work.

Appendix. Supplementary data

Supplementary data associated with this article can be found, in the online version, at doi:10.1016/j.dyepig.2011.05.029.

References

[1] Bordeau G, Lartia R, Teulade-Fichou M-P. meta-Substituted triphenylamines as new dyes displaying exceptionally large stokes shifts. Tetrahedron Lett 2010;51:4429–32.
[2] Wu WC, Yeh HC, Chan LH, Chen CT. Red organic light-emitting diodes with a non-doping amorphous red emitter. Adv Mater 2002;14:1072–5.
[3] Wang JL, Zhou Y, Li YF, Pei J. Solution-processable gradient red-emitting π-conjugated dendrimers based on benzothiadiazole as core: synthesis, characterization, and device performances. J Org Chem 2009;74:7449–56.
[4] J-Thomas KR, Lin JT, Tao YT, Chuen C-H. Star-shaped thieno-[3,4-*b*]-pyrazines: a new class of red-emitting electroluminescent materials. Adv Mater 2002;14:822–6.
[5] Li JY, Liu D. Dendrimers for organic light-emitting diodes. J Mater Chem 2009;19:7584–91.
[6] Liu D, Ren HC, Li JY, Tao Q, Gao ZX. Novel perylene bisimide derivative with fluorinated shell: a multifunctional material for use in optoelectronic devices. Chem Phys Lett 2009;482:72–6.
[7] Hamada Y, Kanno H, Tsujioka T, Takahashi H, Usuki T. Red organic light-emitting diodes using an emitting assist dopant. Appl Phys Lett 1999;75:1682–4.
[8] Yang Y, Zhou Y, He QG, He H, Yang CH, Bai FL, et al. Solution-processable red-emission organic materials containing triphenylamine and benzothiadiazole units: synthesis and applications in organic light-emitting diodes. J Phys Chem B 2009;113:7745–52.
[9] Karstens T, Kobs K. Rhodamine B and rhodamine 101 as reference substances for fluorescence quantum yield measurements. J Phys Chem 1980;84:1871–2.
[10] Yuan WZ, Lu P, Chen SM, Lam JWY, Wang ZM, Liu Y, et al. Changing the behavior of chromophores from aggregation-caused quenching to aggregation-induced emission: development of highly efficient light emitters in the solid state. Adv Mater 2010;22:2159–63.
[11] Chen S, Xu XJ, Liu YQ, Yu G, Sun XB, Qiu WF, et al. Synthesis and characterization of n-type materials for non-doped organic red-light-emitting diodes. Adv Funct Mater 2005;15:1541–6.
[12] Tonzola CT, Alam MM, Kaminsky W, Jenekhe SA. New n-type organic semiconductors: synthesis, single crystal structures, cyclic voltammetry, photophysics, electron transport, and electroluminescence of a series of diphenylanthrazolines. J Am Chem Soc 2003;125:13548–58.
[13] Zhu Y, Alam MM, Jenekhe SA. Regioregular head-to-tail poly(4-alkylquinoline)s: synthesis, characterization, self-organization, photophysics, and electroluminescence of new n-type conjugated polymers. Macromolecules 2003;36:8958–68.
[14] Casalbore-Miceli G, Esposti AD, Fattori V, Marconi G, Sabatini C. A correlation between electrochemical properties and geometrical structure of some triarylamines used as hole transporting materials in organic electroluminescent devices. Phys Chem Chem Phys 2004;6:3092–6.
[15] Carroll WR, Pellechia P, Shimizu KD. A rigid molecular balance for measuring face-to-face arene–arene interactions. Org Lett 2008;10:3547–50.
[16] Roncali J. Synthetic principles for bandgap control in linear π-conjugated systems. Chem Rev 1999;97:173–205.
[17] Shahid M, Ashraf RS, Klemm E, Sensfuss S. Synthesis and properties of novel low-band-gap thienopyrazine-based poly(heteroarylenevinylene)s. Macromolecules 2006;39:7844–53.
[18] Kwong RC, Sibley S, Dubovoy T, Baldo M, Forrest SR, Thompson ME. Efficient, saturated red organic light emitting devices based on phosphorescent platinum(II) porphyrins. Chem Mater 1999;11:3709–13.